Research Square

Preprints are preliminary reports that have not undergone peer review.
They should not be considered conclusive, used to inform clinical practice,
or referenced by the media as validated information.

Patient-derived organoid mixed hollow-solid phenotypes associate with drug response and worse clinical outcome in muscle-invasive bladder cancer

Marianna Kruithof-de Julio
marianna.kruithofdejulio@unibe.ch
Urology Research Laboratory
Haiyan Yue
Urology Research Laboratory
Catarina Macedo Silva
Urology Research Laboratory
Martina Radic
Urology Research Laboratory
Marc Zimmerli
Urology Research Laboratory
George N Thalmann
Department of Urology, Inselspital
Beat Roth
Department of Urology, Inselspital
Roland Seiler
Hospital Centre Biel, Urology
Bernhard Kiss
Lindenhofspital
Panagiotis Chouvardas
Urology Research Laboratory

Article

Keywords: Patient-derived organoids; morphology; drug screening; precision medicine

Posted Date: November 9th, 2026

DOI: https://doi.org/10.21203/rs.3.rs-11085769/v1

License: This work is licensed under a Creative Commons Attribution 4.0 International License.
Read Full License

Additional Declarations: No competing interests reported.

Patient-derived organoid mixed hollow-solid phenotypes associate with drug response and worse clinical outcome in muscle-invasive bladder cancer

Haiyan Yue[1]*, Catarina Macedo-Silva[1]*, Martina Radic[1], Marc Zimmerli[1], George N. Thalmann[2], Beat Roth [2], Roland Seiler[1, 2, 3], Bernhard Kiss [2,4], Panagiotis Chouvardas [1,2], Marianna Kruithof-de Julio [1,2,5]

Affiliations:

[1]Urology Research Laboratory, Department for BioMedical Research, University of Bern, 3008 Bern, Switzerland

[2]Department of Urology, Inselspital, Bern University Hospital, University of Bern, 3008 Bern, Switzerland

[3]Hospital Centre Biel, Urology, Biel, Switzerland.

[4]Lindenhofspital Bern, Switzerland.

[5]Translational Organoid Resource, Department for BioMedical Research, University of Bern, 3008 Bern, Switzerland

*Equally contributed authors

Corresponding author: Prof. Dr. Marianna Kruithof-de Julio

To whom correspondence should be addressed, at:

Urology Research Laboratory

Department of BioMedical Research

University of Bern

Murtenstrasse 24, 3008 Bern, Switzerland

Email: marianna.kruithofdejulio@unibe.ch

Abstract

Muscle-invasive bladder cancer (MIBC) is marked by histological and molecular heterogeneity, leading to recurrence and therapy resistance. Current management relies on stage, grade, and performance status, yielding broad treatment categories and a “one-size-fits-all” approach that lacks personalization. Patient-derived organoids (PDOs) preserve parental tumor complexity and offer realistic platforms for drug screening and precision medicine. In this study, fresh MIBC specimens were collected from surgical resections. Established PDOs were classified by bright-field morphology (solid, hollow, mixed) and screened against standard chemotherapies and selected FDA-approved agents (tyrosine kinase, mTOR, and PARP inhibitors, as repurposing candidates). Viability was measured using CellTiter-Glo. PDOs exhibited distinct morphologies. Mixed solid-hollow structures correlated with shorter progression-free survival and a broadly resistant drug-response profile across tested compounds, a pattern replicated in an independent cohort. Overall, a simple microscopy-based PDO phenotyping may provide a rapid, accessible functional layer to complement conventional clinicopathological stratification in MIBC. Integrating morphology with organoid drug screening offers a scalable platform for biomarker discovery and hypothesis generation, warranting validation in larger, independent cohorts.

Abbreviations: Patient-derived organoids; morphology; drug screening; precision medicine

Introduction

Bladder cancer (BLCa) is a common malignant tumor of the urinary system and a significant global health burden, ranking ninth in incidence and thirteenth in cancer-related mortality worldwide (1). Based on whether the tumor invades the muscularis propria of the bladder wall, BLCa can be classified as non-muscle-invasive bladder cancer (NMIBC) or muscle-invasive bladder cancer (MIBC) (2, 3). Although MIBC accounts for approximately 25% of newly diagnosed bladder cancers, its heterogeneous biology contributes to an aggressive clinical course marked by progression, recurrence, and metastasis (3, 4). Despite multimodal treatment strategies centered on radical cystectomy (RC) combined with neoadjuvant or perioperative systemic therapy (2, 3, 5, 6), many patients still derive limited benefit from initial treatment, with clinical studies showing that close to 50% of patients do not respond adequately (7, 8). Therefore, a deeper understanding and optimization of treatment strategies for MIBC is crucial for improving the overall prognosis of BLCa.

Given this background, a major barrier to improving treatment outcomes in MIBC is the lack of clinically relevant models and biomarkers that capture the biological heterogeneity underlying differences in tumor behavior, clinical risk, and therapeutic response. Conventional clinicopathological classification, including TNM staging, primarily reflects the anatomical extent of disease, but does not capture the biological heterogeneity that influences tumor behavior and therapeutic response. Patient-derived organoids (PDOs) provide a promising platform to address this limitation. PDOs can retain key histological and molecular characteristics of parental tumors (PTs) while enabling functional assessment of therapeutic responses *ex vivo* (9, 10). Therefore, PDO-based approaches offer an opportunity to identify patient-specific tumor states associated with clinical outcomes and patterns of therapeutic vulnerability.

To address this need, we established a patient-derived organoid (PDO) biobank from MIBC cystectomy samples and performed multi-drug functional screening in established PDO cultures. This platform can capture key biological characteristics of PTs and generate patient-specific functional readouts of therapeutic response across multiple compounds (9-11). In addition to functional drug testing, PDO morphology provides a rapid and accessible phenotypic representation of tumor state.

We therefore investigated whether morphological PDO phenotypes were associated with clinical behavior and drug-response profiles, with the aim of evaluating morphology as a potential stratification biomarker.

Results

Study design and integrated workflow for PDO phenotyping and drug screening

We established a short-term MIBC-PDO platform that enabled morphological phenotyping and *ex vivo* drug-response profiling within a timeframe compatible with postoperative clinical decision-making. The integrated workflow is outlined in Figure 1 and comprised tumor biobanking, PDO generation, morphological assessment, and drug screening. Fresh tumor specimens obtained at radical cystectomy, including samples from treatment-naive

patients and patients previously exposed to neoadjuvant chemotherapy, were used to generate PDO cultures, while matched material was retained for histopathological and molecular analyses.

PDOs formed within 7–14 days and were classified according to their morphological features before functional profiling. Established cultures were subsequently expanded for comprehensive drug screening, allowing quantitative assessment of viability following exposure to selected compounds. This workflow provided paired morphological and pharmacological phenotypes for downstream comparison with clinicopathological and molecular features.

Efficient establishment of short-term MIBC PDOs reveals distinct morphological phenotypes

Our short-term MIBC PDO culture system was successfully established from 60 out of 70 tumor specimens, corresponding to an organoid-forming efficiency of 85.7% (Figure 2A). Unsuccessful samples were primarily due to insufficient viable cells after digestion or severe fungal contamination. Consistent with our previous study (9), representative immunofluorescence staining showed that short-term MIBC PDOs retained key molecular characteristics of their matched parental tumors, with consistent expression patterns of classical epithelial, basal, luminal, and proliferation markers (E-cadherin, CK5, p63, CK8, and Ki67; Figure 2B).

Among successfully established PDOs, solid and mixed morphologies - the latter defined by the coexistence of solid and hollow structures within the same culture - were the predominant phenotypes (Figure 2C). Specifically, 30 PDOs (50.00%) exhibited a solid morphology, while 29 (48.33%) displayed a mixed phenotype (Figure 2C). Only 1 sample (1.67%) presented hollow organoid structures (Figure 2C).

Representative bright-field images illustrate three main morphological categories of PDOs (Figure 2D): solid, hollow, and mixed structures. Solid organoids consisted of densely packed cells without visible luminal cavities and displayed a defined outer boundary. In contrast, hollow organoids consisted of well-defined cavities lined by a thin epithelial layer and lacked solid components. This morphology was underrepresented in our MIBC cohort. The third morphological category, mixed organoids, contained coexisting solid and hollow regions within the same structure. This category included budding organoids, in which hollow regions protruded from solid structures, as well as hybrid forms with variable proportions of solid and hollow components.

Mixed PDO morphology was associated with a broad drug resistance profile in MIBC

Building on our previous exploratory work (9), we screened early-passage PDOs from 22 MIBC samples with a panel of FDA-approved drugs, including standard-of-care agents and candidates selected for their clinical relevance and repurposing potential. Drug-response profiling revealed substantial heterogeneity at both the intra-individual and inter-individual levels (Figure 3A, B). In the heatmap of vehicle-normalized z-scores (Figure 3A), responses to the targeted compounds varied markedly across PDOs, suggesting that drug sensitivity was driven by underlying tumor biology rather than a uniform response pattern. Responses to chemotherapy combinations were generally more effective, but also heterogeneous across PDOs. For example, in BLCa-185, the cisplatin-gemcitabine combination did not improve the response compared with monotherapy (Figure 3A). Although this combination showed an overall

effect across the cohort, when normalized to the vehicle (Figure 3A), cross-sample analysis identified both highly responsive and poorly responsive PDOs (Figure 3B). Similarly, the MVAC regimen (Methotrexate, Vinblastine, Doxorubicin and Cisplatin) did not consistently outperform Doxorubicin monotherapy, and responses to its individual components varied across samples (Figure 3A). These findings highlight the potential of PDO-based functional screening to identify patient-specific therapeutic vulnerabilities beyond population-level response patterns.

To determine whether the observed variability in drug response was associated with PDO morphology, we next compared drug sensitivity profiles between solid and mixed PDOs (Figure 3C). Mixed PDOs showed higher compound-normalized mean z-scores than solid PDOs across most chemotherapeutic and targeted agents, yielding predominantly positive Δ mean z-scores (mixed minus solid) and indicating relative drug resistance of the mixed phenotype. This pattern was observed across all four drug classes. Several compounds, including paclitaxel, epirubicin, and selected tyrosine kinase inhibitors, showed significantly higher resistance in mixed than in solid PDOs. Additionally, this morphology-associated drug-response pattern was independently supported in a second, previously published PDO cohort (9), in which the same analysis showed a consistent trend and statistically significant differences between solid and mixed PDOs (Supplementary Figure 1).

These results suggest that PDO morphology captures a phenotypic dimension of tumor heterogeneity that is functionally associated with treatment response and may contribute to morphology-informed PDO-guided treatment stratification in MIBC.

Mixed PDO morphology was associated with worse progression-free survival in MIBC

We further assessed the association between PDO morphology and clinical outcome. The solid and mixed PDO morphologies were descriptively examined in relation to clinical stage (AJCC) and pathological T stage after neoadjuvant chemotherapy at cystectomy. Most samples were classified as AJCC stage III and stage T3, with comparable numbers of solid PDOs (Supplementary Figure 2A, B). Stage II and IV groups contained few samples, precluding inference regarding stage-dependent differences (Supplementary Figure 2A, B). Although solid PDOs appeared more frequent with increasing T stage, the small sample sizes within individual T-stage categories limit interpretation.

Kaplan-Meier analysis of recurrence-free survival (RFS), stratified by PDO morphology, showed a significant difference between the solid and mixed groups ($p=0.0083$; Figure 4). Patients whose PDOs displayed a solid morphology had a higher probability of RFS, whereas those with mixed PDOs showed a more rapid decline in RFS. In contrast, disease-specific survival did not differ significantly between the two morphological groups (Supplementary Figure 2C).

Together, these findings suggested that mixed PDO morphology is associated with a higher risk of disease progression and recurrence.

Discussion

Despite advances in the clinical management of MIBC, treatment selection remains insufficiently individualized, highlighting the need for patient-specific models and biomarkers that can inform therapeutic decision-making. Although tumor heterogeneity is a key determinant of treatment response, clinical decision-making still relies largely on anatomical staging and a limited number of molecular markers, with few functional tools to translate tumor heterogeneity into treatment selection (2, 3, 5, 6, 12-17).

Drug repurposing offers an opportunity to broaden therapeutic options using agents with existing clinical safety and pharmacokinetic data, potentially accelerating their translation into MIBC treatment (9, 10, 18, 19). However, the expanding number of available compounds, particularly multi-target TKIs, also increases the complexity of selecting the most appropriate treatment for an individual patient. This challenge is intensified by marked inter-patient tumor heterogeneity and the limited availability of functional tools that can guide drug selection.

To address this need, we established an integrated workflow combining rapid PDO generation and high-throughput drug screening. This approach was designed both to functionally identify patient-specific drug sensitivities and to address functional features that may predict response before functional testing.

Using this framework, PDO morphology emerged as a clinically accessible first-layer biomarker that broadly stratified tumor aggressiveness and drug responsiveness. Specifically, we found that a mixed-morphological phenotype was associated with an increased risk of disease progression and consistently showed poorer responses across drug screening assays, both chemotherapeutics and targeted therapies. This broadly resistant drug-response pattern was also observed in an independent cohort from our previous study, supporting the reproducibility of the association.

To our knowledge, this is the first study in BlCa associating PDO morphology states with functional and clinical outcomes. Nonetheless, our findings partially align with observations in other tumor types. In pancreatic ductal adenocarcinoma, early morphological classification of PDOs into gland-like versus densely proliferating types recapitulated molecular subtypes and predicted chemotherapy response and overall survival (20). In a second study, in colorectal cancer, time-resolved, multi-parametric morphological readouts from PDOs (aggregated morphological indicators derived from optical coherence tomography) correlated strongly with ATP-based viability and captured drug-response heterogeneity across treatments (21).

PDO-based drug screening is increasingly recognized as a powerful tool to capture patient-specific drug sensitivities *in vitro* within clinically relevant timeframes and is being actively evaluated in multiple ongoing trials (22, 23). Our findings support further evaluation of PDO morphology as a simple, rapid phenotypic readout alongside functional drug testing, an accessible tool that could be readily integrated into standard workflows to guide initial therapeutic choices while more detailed molecular or functional assays are still pending. However, the present observations are exploratory and require validation in larger, independent and prospectively collected MIBC cohorts. Future work

may also investigate whether integrating morphology with additional clinical or molecular variables improves the reproducibility and clinical relevance of morphology-based stratification.

Study Limitations

The following limitation should be considered when interpreting the results. Our analyses are based on a relatively small, single-center MIBC cohort, and only a subset of tumors yielded PDOs with sufficient growth and viability for drug screening. This introduces potential selection bias, as the tumors that can be successfully expanded *in vitro* may not fully represent the broader MIBC population, which could limit the generalizability of our findings.

Materials and methods

Cohort description and ethics

All the patients included in this study were treated and followed up at the Department of Urology at Insel University Hospital, Bern, Switzerland, and the Department of Urology at Spitalzentrum Biel / Centre hospitalier Bienne, Biel/Bienne, Switzerland between 2020-2025. All data were treated according to the protocol approved by Ethical Committee Bern (Cantonal Ethical approval KEK 06/03 and 2017-02295). All research was performed in accordance with relevant guidelines and regulations, in line with the principles of the Declaration of Helsinki. Written informed consent was obtained from each patient included in the study.

A total of 70 fresh MIBC tumor specimens, with matched peripheral-blood samples where available, were prospectively collected for biobanking from patients undergoing radical cystectomy at Inselspital, University Hospital of Bern, or Spitalzentrum Biel/Centre hospitalier Bienne. These specimens were used for PDO derivation. Clinical and pathological characteristics were appropriately available for 36 patients, who constituted the cohort for analyses of associations between PDO phenotypes and clinical outcomes. Clinical and pathological characteristics are summarized in supplementary table 1 and table 2. Of these, 22 matched PDO cultures derived drug-screening data.

Sample collection and processing

Tumor tissues from cystectomies from patients diagnosed with MIBC were collected in the operating room, immediately after resection, in a collection medium that contains DMEM medium (Thermo Fisher Scientific, 61965-026),100 µg/ml Primocin (InVivoGen, ant-pm-2), and 2.5 µg/ml Fungizone. Usually, the entire tissue processing procedure does not exceed 2 hours to avoid inherent tissue damage.

Whenever possible, organoid derivation was done by digesting the tissues in fresh. Then, in parallel to the organoid derivation, the workflow of sample processing at the lab includes tissue cryopreservation in freezing medium, which contains 90% Calf Serum (sigma C8056) with 10% Dimethyl sulfoxide (DMSO, Thermo Fisher Scientific, J66650.AK) at -150ºC for long-term preservation. Lastly, one to two representative tumor pieces were selected for histological

analysis. Briefly, tissues were washed in PBS 1x for 15min at room temperature (RT). Then, 4% PFA was added for fixation at 4 °C, overnight, in rotation. The day after, the sample was washed three times in PBS 1x at RT for 10min, in rotation. Then, 50% EtOH was added, and the sample was stored at 4 °C for further tissue embedding and histological analysis. Specifically, the fixed tissue was transferred from 50% to 70% ethanol and incubated at 4 °C for 3-5 hours as a pre-treatment before embedding. We then used the Leica HistoCore PEARL tissue processor, an automatic gradient dehydration system, to dehydrate the samples. This was followed by paraffin embedding using the Leica HistoCore Arcadia H/C. After embedding, the specimens were cooled to room temperature and stored at 4 °C overnight before sectioning.

Tissue digestion and organoid derivation

Organoid derivation was done from fresh or cryopreserved tissues. The tissue was centrifuged at 700 × g for 5 minutes at RT. Then, washing medium containing 0.2% Bovine serum albumin (BSA, Sigma-Aldrich, A1470-25G), 1X Pen/Strep (Thermo Fisher Scientific, 15140122), and HBSS (Thermo Fisher Scientific, 14175129) was used to wash it at least once (up to twice for cryopreserved tissue). The tissue samples were then cut into small pieces of around 2 mm^3, placed in the basic medium (Advanced DMEM/F12 Medium Thermo Fisher Scientific,12634-010), 2 mM GlutaMAX supplement (Thermo Fisher Scientific, 35050061), 10 mM HEPES (Thermo Fisher Scientific, 3.259.408,00), and 100 µg/ml Primocin (InVivoGen, ant-pm-2), and centrifuged at 700 × g, 5 min at RT.

Subsequently, 5 mg/ml collagenase II (Thermo Fisher Scientific, 3298433) in the basic medium, supplemented with 15 µg/ml DNase I (Zymo Research, E1010), and 10 µM Y-27632-HCl ROCK inhibitor (Selleck Chemicals, S1049) was used for 1-2 hours at 37 °C in a water bath with shaking for tissue digestion. Mechanical dissociation by repeated pipetting was performed throughout this period until no visible tissue fragments remained.

If there were still many cell clusters mixed in it after this period, the pellet was centrifuged at 700 × g, 5 min at RT, resuspend in 2-4 ml TrypLE Express (Thermo Fisher Scientific, 12605028) and incubated at 37 °C for 5-10 min. Afterward, the pellet was incubated in 1 mL cold EC lysis buffer for 1 min at room temperature and then washed with 5 mL washing medium (700 × g, 5 min, RT), which can be skipped if no obvious red blood cell contamination is observed. Then the cell suspension was filtered through a 70 µm cell strainer (pluriselect, 43-50070-51) to remove the fibers inside.

Later, cells were washed in the basic medium (300 g, 5 min) and counted. Then the cell pellet was resuspended in Human BlCa organoid medium and was seeded in ultra-low attachment (ULA) plates (Corning, 3471). Generally, 500,000-1000,000 cells were seeded per well in 6-well plates in 1.5-2 ml of Human BlCa organoid medium. Organoids were incubated at 37 °C with 5% CO_2. Human BLCa organoid medium composition is detailed in supplementary table 3.

Drug screening assay

Within 1 to 2 weeks of organoid culture, the respective organoids formed were collected by centrifugation at 180-220 g for 5 min at RT. Then the organoids were dissociated into single cells with TrypLE Express at 37 °C for 6-12 min. Single cell suspension was counted, washed once in the basic medium (300 × g, 5 min, RT), and resuspended in Human BLCa organoid medium. Then, cells were seeded in a ULA-384 well plate (Corning, cat. no. 4588) with at least 4 technical replicates per treatment group, at a density of 5,000-10,000 cells per well.

After 48 h of culture, the organoids were reformed. After that, the selected compounds or the respective vehicles were added to the culture system to reach the desired final concentration (detailed concentrations are listed in the supplementary Table 4).

After 48 hours of drug treatment, CellTiter-Glo 3D assay (Promega, G9683) was used to measure cell viability, according to the manufacturer's instructions. Additionally, a confocal quantitative image cytometer (CQ1) was used to visualize morphological alterations in organoids before and after treatment, in bright-field images.

Multiplexed Immunofluorescence staining

Formalin-fixed paraffin-embedded (FFPE) tissue blocks were sectioned at 4 µm thickness by using a Thermo Fisher Scientific Microm HM 325 rotary microtome. FFPE sections were deparaffinized in xylene and rehydrated through a graded ethanol series (100%, 94%, and 70%) followed by distilled water (dH2O).

After that, the FFPE sections were transferred into pre-heated citrate-based antigen retrieval buffer (pH 6, cat no.) and boiled in a pressure cooker for 10 minutes. Then, the sections were blocked for 60 min at RT in a blocking buffer containing 1% BSA in PBST (0.1% Tween-20). Then, the blocked sections were incubated in prepared primary antibody solution at proper dilutions in the blocking buffer, and kept at 4 °C overnight. Detailed information on the antibodies is provided in supplementary Table 5.

After primary antibody incubation, sections were incubated at RT for 90 min with the secondary fluorescent antibody.

Then, the sections were incubated in a solution of TO-PRO-3 or DAPI diluted in PBS for 15 minutes or 1 hour for nuclei detection. After that, the slice was mounted using ProLong™ Diamond Antifade Mountant (Thermo Fisher Scientific, P36970) for longer staining preservation. The stained sections were left at RT overnight and scanned using CQ1.

Statistical analysis

All data were analyzed using GraphPad Prism software version 11.0.0. Differences in drug-response z-scores between solid and mixed PDOs across the tested compounds were assessed using two-way analysis of variance (ANOVA), followed by multiple-comparison testing to compare the mean response of mixed versus solid PDOs for each compound. Statistical significance was assessed using a two-tailed test. The corresponding *p value* was reported. ns, not statistically significant; * p<0.05; ** p<0.01; ***p<0.001;****p<0.0001.

Cell viability values were normalized to vehicle-treated controls and expressed as percentage viability. Dose-response curves were generated using log-transformed drug concentrations and analyzed using nonlinear regression with the "log(inhibitor) vs. normalized response - variable slope" model. IC50 values and corresponding 95% confidence intervals were calculated from the fitted dose-response curves.

For drug sensitivity heatmap generation raw counts were normalized independently for each screened sample using the following formula:

X_s=technical replicates for each drug treatment

X_v= mean of technical replicates of the matching vehicle/control conditions

SD_v= standard deviation of the technical replicates of the matching vehicle/control conditions

Norm.X_s= raw counts normalized to the matching vehicle (norm.X_s= X_s/X_v)

X_d= mean of the normalized technical replicates for the specific drug across samples

SD_d= standard deviation of the normalized technical replicates for the specific drug across samples

Z-scores of cisplatin, gemcitabine, daunorubicin, and the combination of cisplatin and gemcitabine were generated using the untreated group as a control, while z-scores of all remaining drugs were generated using DMSO as a control. Raw counts were also used to calculate fold-changes relative to the average of the control raw values.

Acknowledgments

We thank all the patients that participated in our study, as well as all the involved surgical teams and study nurses. This project received funding from Wilhelm Sander-Stiftung, Förderantrags Nr. 2022.136.1 awarded to M. K. d. J., and 3RCC Kompetenzzentrum Schweiz, OC-2019-003 awarded to M. K. d. J.
H.Y PhD was supported by ISREC TANDEM call, CCP 10-3224-9 awarded to B.K and M. K. d. J.

Author's Contribution

HY: data acquisition, data analysis, and original manuscript draft; CMS: conceptualization, data acquisition, data analysis, and original manuscript draft; MR: data acquisition and data analysis; MZ: data acquisition and data analysis; GNT: manuscript revision; BR: manuscript revision; RS: human tumor-sample acquisition, patient-data handling, and manuscript revision; BK: human tumor-sample acquisition, patient-data handling, and manuscript revision; PC: conceptualization, supervision, data analysis and manuscript revision; MKdJ: conceptualization, supervision, and manuscript revision. All authors reviewed and approved the final manuscript.

Declaration of interests

The authors declare no competing interests.

Data availability statement

All data generated or analyzed during this study are included in this article and its supplementary information files. This includes patient-derived organoid (PDO) generation protocols, drug-screening summary data, representative staining images, and the statistical analyses supporting the associations with clinical outcomes. Due to patient privacy and ethical restrictions, raw patient-level data cannot be made publicly available. De-identified data may be shared upon reasonable request from qualified researchers, subject to approval by the Ethics Committee of Bern. Requests should be directed to the corresponding author.

References

1. WHO I. GLOBOCAN 2022: Bladder Cancer. 2022.
2. European Association of U. EAU Guidelines on Non-muscle-invasive Bladder Cancer. Arnhem, The Netherlands: European Association of Urology; 2026.
3. European Association of U. EAU Guidelines on Muscle-invasive and Metastatic Bladder Cancer. Arnhem, The Netherlands: European Association of Urology; 2026.
4. Burger M, Catto JW, Dalbagni G, Grossman HB, Herr H, Karakiewicz P, et al. Epidemiology and risk factors of urothelial bladder cancer. Eur Urol. 2013;63(2):234-41.
5. National Comprehensive Cancer N. NCCN Clinical Practice Guidelines in Oncology: Bladder Cancer. Version 1.2026. Plymouth Meeting, PA: NCCN; 2026.
6. National Health Commission of the People's Republic of C. Chinese guidelines for diagnosis and treatment of urothelial carcinoma of bladder 2018 (English version). Chin J Cancer Res.31(1):49-66.
7. Galsky MD, Daneshmand S, Izadmehr S, Gonzalez-Kozlova E, Chan KG, Lewis S, et al. Gemcitabine and cisplatin plus nivolumab as organ-sparing treatment for muscle-invasive bladder cancer: a phase 2 trial. Nat Med. 2023;29(11):2825-34.
8. Necchi A, Anichini A, Raggi D, Briganti A, Massa S, Lucianò R, et al. Pembrolizumab as Neoadjuvant Therapy Before Radical Cystectomy in Patients With Muscle-Invasive Urothelial Bladder Carcinoma (PURE-01): An Open-Label, Single-Arm, Phase II Study. J Clin Oncol. 2018;36(34):3353-60.
9. Minoli M, Cantore T, Hanhart D, Kiener M, Fedrizzi T, La Manna F, et al. Bladder cancer organoids as a functional system to model different disease stages and therapy response. Nat Commun. 2023;14(1):2214.
10. Merrill NM, Kaffenberger SD, Bao L, Vandecan N, Goo L, Apfel A, et al. Integrative Drug Screening and Multiomic Characterization of Patient-derived Bladder Cancer Organoids Reveal Novel Molecular Correlates of Gemcitabine Response. Eur Urol. 2024;86(5):434-44.
11. Thorel L, Perréard M, Florent R, Divoux J, Coffy S, Vincent A, et al. Patient-derived tumor organoids: a new avenue for preclinical research and precision medicine in oncology. Experimental & Molecular Medicine. 2024;56(7):1531-51.

12. Comprehensive molecular characterization of urothelial bladder carcinoma. Nature. 2014;507(7492):315-22.
13. Kamoun A, de Reyniès A, Allory Y, Sjödahl G, Robertson AG, Seiler R, et al. A Consensus Molecular Classification of Muscle-invasive Bladder Cancer. Eur Urol. 2020;77(4):420-33.
14. Sjödahl G, Lauss M, Lövgren K, Chebil G, Gudjonsson S, Veerla S, et al. A molecular taxonomy for urothelial carcinoma. Clin Cancer Res. 2012;18(12):3377-86.
15. Lindgren D, Frigyesi A, Gudjonsson S, Sjödahl G, Hallden C, Chebil G, et al. Combined gene expression and genomic profiling define two intrinsic molecular subtypes of urothelial carcinoma and gene signatures for molecular grading and outcome. Cancer Res. 2010;70(9):3463-72.
16. Lee HW, Chung W, Lee HO, Jeong DE, Jo A, Lim JE, et al. Single-cell RNA sequencing reveals the tumor microenvironment and facilitates strategic choices to circumvent treatment failure in a chemorefractory bladder cancer patient. Genome Med. 2020;12(1):47.
17. Robertson AG, Kim J, Al-Ahmadie H, Bellmunt J, Guo G, Cherniack AD, et al. Comprehensive Molecular Characterization of Muscle-Invasive Bladder Cancer. Cell. 2017;171(3):540-56.e25.
18. Ioakeim-Skoufa I, Tobajas-Ramos N, Menditto E, Aza-Pascual-Salcedo M, Gimeno-Miguel A, Orlando V, et al. Drug Repurposing in Oncology: A Systematic Review of Randomized Controlled Clinical Trials. Cancers (Basel). 2023;15(11).
19. Al Khzem AH, Gomaa MS, Alturki MS, Tawfeeq N, Sarafroz M, Alonaizi SM, et al. Drug Repurposing for Cancer Treatment: A Comprehensive Review. Int J Mol Sci. 2024;25(22).
20. Matsumoto K, Fujimori N, Ichihara K, Takeno A, Murakami M, Ohno A, et al. Patient-derived organoids of pancreatic ductal adenocarcinoma for subtype determination and clinical outcome prediction. J Gastroenterol. 2024;59(7):629-40.
21. Zhang L, Wang L, Yang S, He K, Bao D, Xu M. Quantifying the drug response of patient-derived organoid clusters by aggregated morphological indicators with multi-parameters based on optical coherence tomography. Biomed Opt Express. 2023;14(4):1703-17.
22. Seiler R, Egger M, De Menna M, Wehrli S, Minoli M, Radić M, et al. Guidance of adjuvant instillation in intermediate-risk non-muscle invasive bladder cancer by drug screens in patient derived organoids: a single center, open-label, phase II trial. BMC Urol. 2023;23(1):89.
23. Yue H, Carchidi D, Schmucker P, Seiler R, Kiss B, Macedo-Silva C, et al. Clinical Translation of Patient-Derived Organoids: Perspectives for Personalized Therapy in Cancer. Int J Cancer. 2026.

Figure legends

Figure 1. Schematic overview of the experimental workflow for short-term patient-derived organoid (PDO) generation and *ex vivo* drug screening in muscle-invasive bladder cancer (MIBC).

(A) Processing and biobanking. Fresh parental tumor (PT) tissue was collected from patients with MIBC undergoing radical cystectomy. Tumor material was stored by cryopreservation, while a representative tissue fragment underwent formalin fixation and paraffin embedding (FFPE) to enable histological analysis (B) Organoid derivation and ex vivo drug screening. Fresh or cryopreserved PT tissue was enzymatically dissociated into single cells. PDO formation and morphology were monitored over 7-14 days. Once established, PDOs were employed for subsequent drug-screening assays. Created in https://BioRender.com.

Figure 2. Morphological characterization of MIBC patient-derived organoids (PDOs) and clinical association.

(A) Pie chart summarizing PDO formation efficiency from all collected samples (n = 70), showing a success rate of 85.71% (60/70) and a failure rate of 14.29% (10/70). (B) Histological comparison between parental tumor tissues and corresponding PDOs using hematoxylin and eosin (H&E) staining. Immunofluorescence (IF) analysis of PDOs showing expression of epithelial and lineage markers, including E-cadherin (epithelial), CK5/p63 (basal markers), CK8 (luminal marker), and Ki67 (proliferation marker). (C) Distribution of PDO morphological phenotypes among successfully established organoids (n = 60), including solid (50.00%, 30/60), mixed (48.33%, 29/60), and hollow (1.67%, 1/60) types. (D) Representative brightfield images of short-term culture PDOs, illustrating three distinct morphological phenotypes: solid, mixed, and hollow structures. Scale bars, 50 μm.

Figure 3. Morphology-associated drug responses in MIBC patient-derived organoids.

PDO drug screening analysis (n = 22 biological samples). The heatmap in (A) reports the average of z-scores normalized to vehicle controls for each biological sample, while (B) Heatmap of drug-specific Z-scores across PDO samples, derived from vehicle-normalized fold changes. Statistical significance between treatments and vehicle controls was assessed using one-way analysis of variance (ANOVA), with multiple-comparison adjustment. Adjusted P values ≤ 0.05 were considered statistically significant. (C) Drug responses were averaged as drug-specific Z-scores. Drug-response differences were evaluated using two-way ANOVA, with PDO morphology (solid versus mixed) and compound as factors. Post hoc multiple-comparison testing was performed by comparing the two cell means within each compound, corresponding to mixed versus solid PDOs for each drug, $p < 0.0001$. For each compound, the mean compound-normalized z-score was calculated separately for mixed and solid PDOs, and the difference was derived as Δ mean z-score = mixed PDO mean z-score − solid PDO mean z-score. Compounds are ordered by Δ mean z-score. Positive values indicate higher relative viability and relative resistance in mixed PDOs, whereas negative values indicate relative sensitivity in mixed PDOs.

Figure 4. PDO phenotype and clinical outcomes.

Kaplan-Meier recurrence-free survival (RFS) analysis stratified by PDO morphology (log-rank test, $p = 0.0083$).

Fig. 1

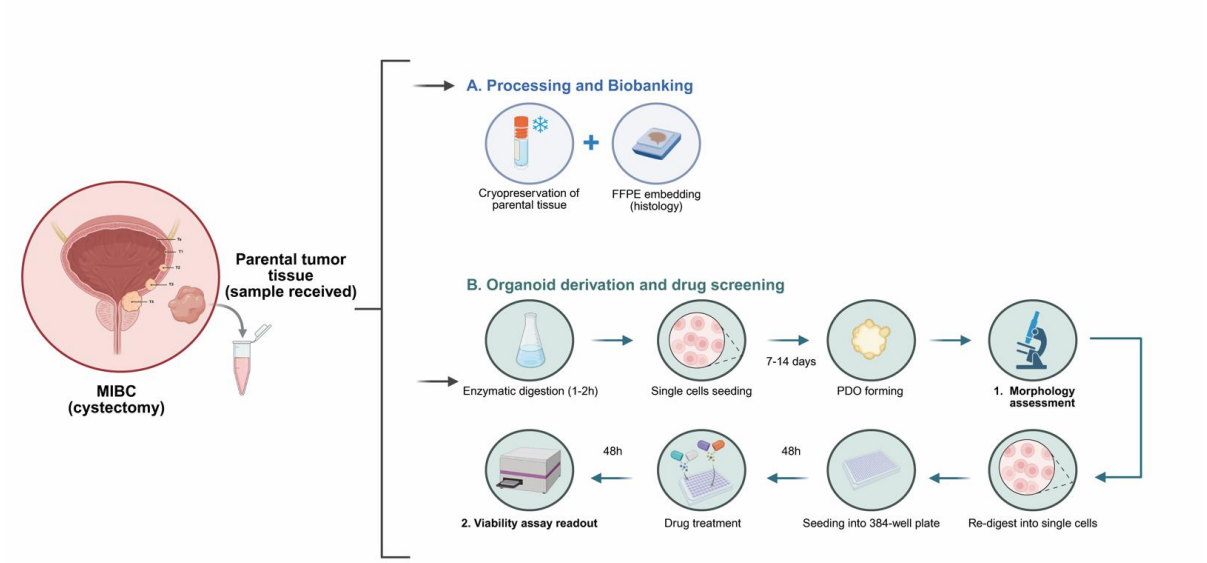
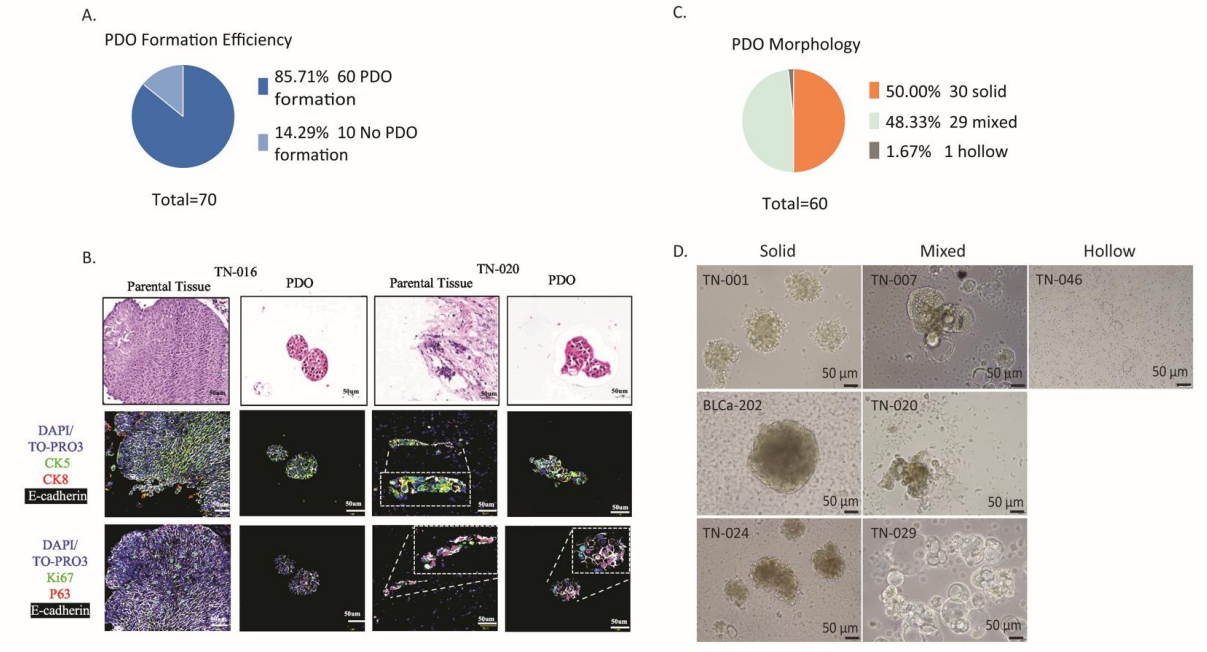
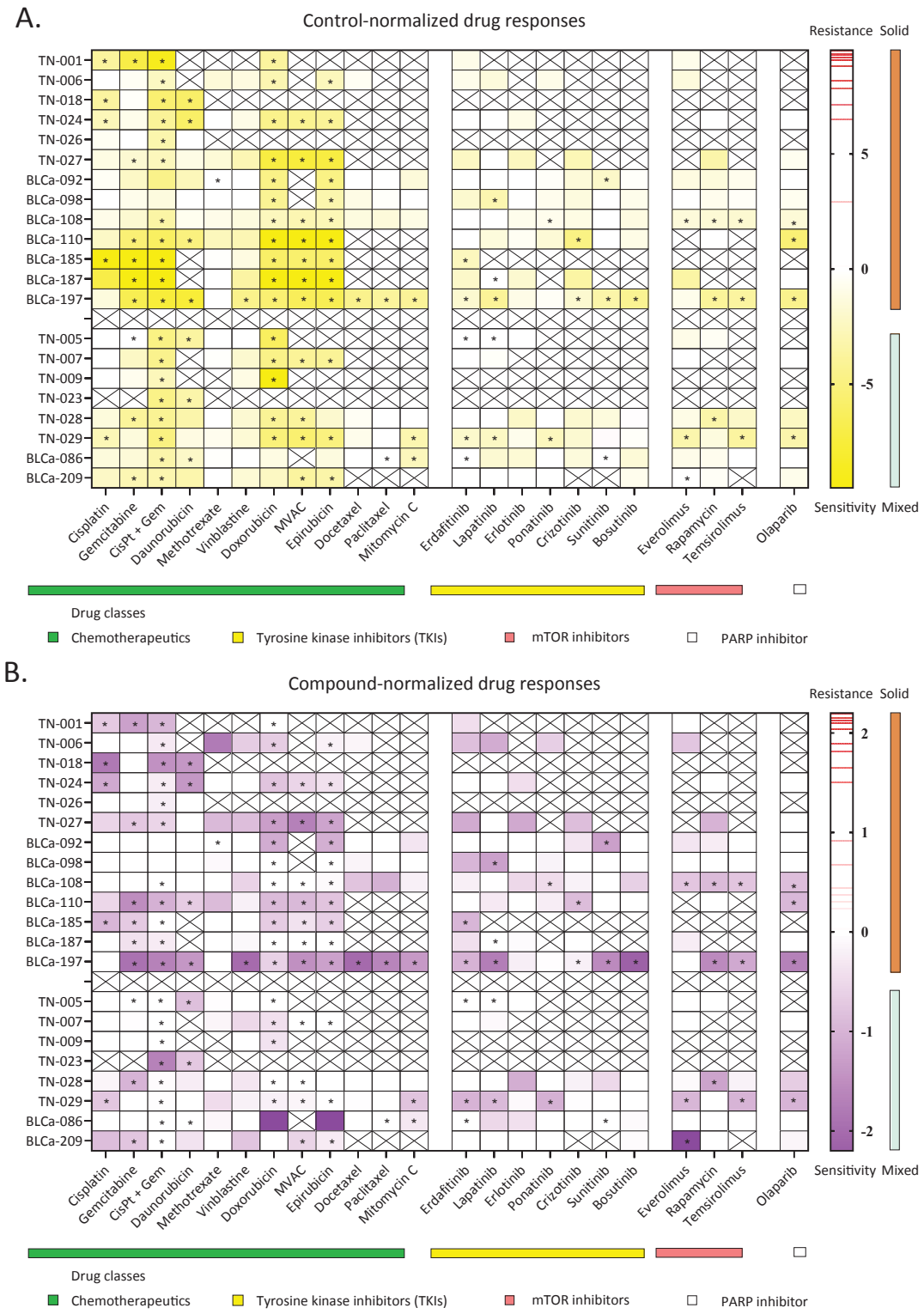
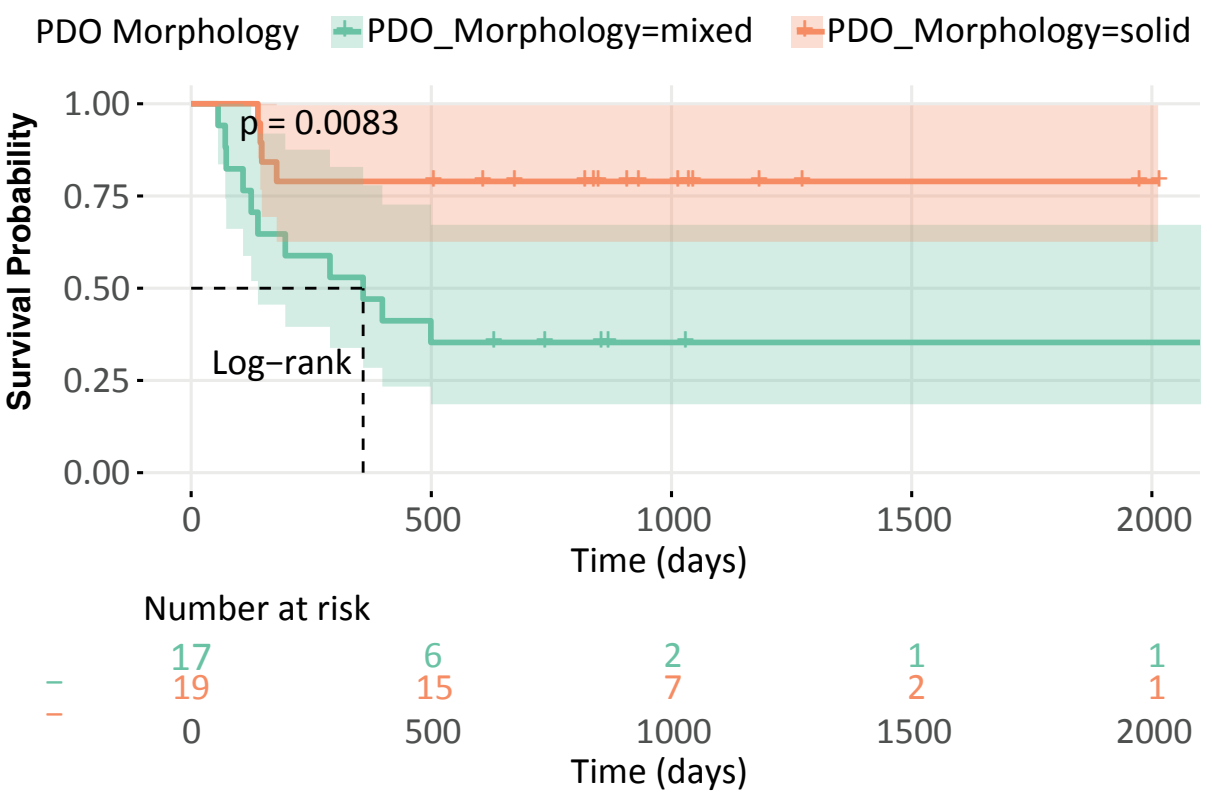

A. Processing and Biobanking
Cryopreservation of parental tissue
FFPE embedding (histology)
Parental tumor tissue (sample received)
MIBC (cystectomy)
B. Organoid derivation and drug screening
Enzymatic digestion (1-2h)
Single cells seeding
7-14 days
PDO forming
1. Morphology assessment
Re-digest into single cells
Seeding into 384-well plate
48h
Drug treatment
48h
2. Viability assay readout

Fig. 2


A.
PDO Formation Efficiency
85.71% 60 PDO formation
14.29% 10 No PDO formation
Total=70
B.
TN-016
Parental Tissue
PDO
TN-020
Parental Tissue
PDO
DAPI/ TO-PRO3
CK5
CK8
E-cadherin
DAPI/ TO-PRO3
Ki67
P63
E-cadherin
C.
PDO Morphology
50.00% 30 solid
48.33% 29 mixed
1.67% 1 hollow
Total=60
D.
Solid
Mixed
Hollow
TN-001
TN-007
TN-046
BLCa-202
TN-020
TN-024
TN-029
50 μm


A.
Control-normalized drug responses
Resistance
Solid
Sensitivity
Mixed
TN-001
TN-006
TN-018
TN-024
TN-026
TN-027
BLCa-092
BLCa-098
BLCa-108
BLCa-110
BLCa-185
BLCa-187
BLCa-197
TN-005
TN-007
TN-009
TN-023
TN-028
TN-029
BLCa-086
BLCa-209
Cisplatin
Gemcitabine
CisPt + Gem
Daunorubicin
Methotrexate
Vinblastine
Doxorubicin
MVAC
Epirubicin
Docetaxel
Paclitaxel
Mitomycin C
Erdafitinib
Lapatinib
Erlotinib
Ponatinib
Crizotinib
Sunitinib
Bosutinib
Everolimus
Rapamycin
Temsirolimus
Olaparib
Drug classes
Chemotherapeutics
Tyrosine kinase inhibitors (TKIs)
mTOR inhibitors
PARP inhibitor
B.
Compound-normalized drug responses
Resistance
Solid
Sensitivity
Mixed
Drug classes
Chemotherapeutics
Tyrosine kinase inhibitors (TKIs)
mTOR inhibitors
PARP inhibitor
C.
PDO drug screening
Daunorubicin
Olaparib
Mathotrexate
Temsirolimus
Erlotinib
Lapatinib
Mitomycin C
cisplatin
Rapamycin
Crizotinib
Vinblastine
Ponatinib
CispPt + Gem
Sunitinib
Gemcitabin
Bosutinib
Everolimus
Docetaxel
MVAC
Erdafitinib
Doxorubicin
epirubicin
Paclitaxel
-0.5
0.0
0.5
1.0
1.5
Δ mean z-score (mixed vs solid)

A.


PDO Morphology
PDO_Morphology=mixed
PDO_Morphology=solid
Survival Probability
1.00
0.75
0.50
0.25
0.00
p = 0.0083
Log−rank
0
500
1000
1500
2000
Time (days)
Number at risk
17
6
2
1
1
19
15
7
2
1
0
500
1000
1500
2000
Time (days)

Supplementary Files

This is a list of supplementary files associated with this preprint. Click to download.

- Sup.Fig.1.pdf
- Sup.Fig.2.pdf